ELECTRICAL CHARACTERIZATION OF GaAs SINGLE CRYSTAL IN DIRECT SUPPORT OF M555 FLIGHT EXPERIMENT

by

J. G. Castle

Final Technical Report

This study was supported by the

Space Sciences Laboratory
National Aeronautics and Space Administration
Marshall Space Flight Center
Marshall Space Flight Center, AL 35812

under Contract NAS8-29542

Department of Physics
School of Graduate Studies and Research
The University of Alabama in Huntsville
Huntsville, AL 35807

September 1975

FTR - NAS8-29542

FINAL TECHNICAL REPORT ON CONTRACT NAS8-29542

TITLE OF CONTRACT: Electrical Characterization of GaAs Single Crystal in Direct Support of M555 Flight Experiment

SUBJECT: Electrical Characterization of Single Crystal Surfaces

PREPARED BY: J. G. Castle, Principal Investigator
Professor of Physics, UAH

ABSTRACT: The exploration of several nondestructive methods of electrical characterization of semiconductor single crystals was carried out during the period ending May 1974. Two methods of obtaining the microwave skin depth, one for the mapping flat surfaces and the other for analyzing the whole surface of small single crystal wafers, were developed to the stage of working laboratory procedures. The preliminary 35 GHz data characterizing the two types of space-related single crystal surfaces, flat slices of gallium arsenide and small wafers of germanium selenide, are discussed. A third method of nondestructive mapping of donor impurity density in semiconductor surfaces by scanning with a light beam was developed for GaAs; its testing, done to a large extent without NASA support, indicates reasonable precision at reasonable scan rates for GaAs surfaces at room temperature.

SUBMITTED TO: Space Sciences Laboratory, ATTN: ES 12
National Aeroanutics and Space Administration
Marshall Space Flight Center
Marshall Space Flight Center, AL 35812

SUBMITTED BY: The University of Alabama in Huntsville
School of Graduate Studies and Research
P. O. Box 1247
Huntsville, AL 35807

September 1975

FOREWORD

The author gratefully acknowledges the many significant contributions of his supporting staff on this remarkably successful project. Gratitude goes: to R. R. Lattanzi, Research Engineer and Paul Zimmerman, Electronic Technician for their careful learning of some microwave techniques,

to James M. Rowe, Graduate Student, for his diligence in the successful optical scanning of GaAs at room temperature

to Michael Valpiani, Senior, for his effective derivation of the algebra and execution of data reduction for the 35 GHz skin effects for this final report and

to Karla Dalton, Sophomore, for her mastery of the programming of the new graphics display terminal so as to display the luminescence spectra automatically,

but any shortcomings in this report rest with the P.I. The reader is warned that NASA's kindness in allowing a one-year, no-cost extension for the purpose of improving the write-up does not guarantee the correctness of the formulae presented herein. The 35 GHz skin depth values were calculated from observed power ratios by the use of these formulae for data reduction and were submitted to the COR early in the summer of '74.

TABLE OF CONTENTS

TABLE OF CONTENTS (Contd)

I. INTRODUCTION

The NASA program for growth of semiconductor single crystals in the space environment of Skylab was expected* to produce crystals of significantly higher quality than attainable through the same growing processes on earth. As the semiconductor crystals become more perfect if undoped or more uniform if doped, the emphasis in any measurement of them shifts increasingly toward care in avoiding damage to the crystal by the measurement.

A. Need for Nondestructive Method for Electrical Characterization

Electrical characterization of a single crystal of semiconductor usually involves "soldering" ohmic contacts in several locations in order to obtain some average bulk property (e.g. bulk resistivity) for the sample piece. Whenever the crystal is to be evaluated for use in large scale integrated (LSI) circuitry, the characterization should include a search for local variations in electrical properties. Such a search should use a nondestructive method of mapping the surface of the semiconductor.

Clearly, the mapping of electrical characteristics of high quality crystals, such as those grown on Skylab flights, should be done without inflicting any damage. To this end, noncontacting methods of mapping were sought - avoiding the formation of "solder" contacts and avoiding the high local pressure of point contacts. In addition to valuable monitoring of NASA's space processed materials, the successful development of suitable noncontacting methods of electrical measurement would be of considerable spinoff value to U. S. semiconductor manufacturers or at least to U. S. semiconductor circuit manufacturers.

---

*This expectation was realized many times in high quality semiconductor crystals grown on the Skylab missions during 1973 and 1974.

B. Noncontacting Techniques for High Quality Single Crystals

The class of techniques by which the electrical properties of a semiconductor single crystal can be observed without contacts is limited to coupling to the crystal by electromagnetic radiation at frequencies from rf to the near uv. The optical frequencies have been used to probe the uniformity of certain types of impurities in semiconductor crystals.[1] A wide range of radiation frequencies can be used to observe the mobilities and the concentrations of the various types of charge carriers present near the surface of the semiconductor cyrstal being examined. For surveying carrier concentrations and mobilities of thin semiconductor sheets, useful measurements of optical transmission and reflection with commercial instruments have been reported[2] with 1.5 mm diameter resolution. In addition, the impurities within the semiconductor can often[3] be identified by X-radiation.

Coupling to a semiconductor at high frequencies implies[4] the reaction of the semiconductor will take place near the surface, i.e., within the "skin depth," δ_s. The "classical" application of Maxwell's equations for the case of a field E_z applied to a plane surface of semi-infinite conductor extending from $x = 0$ gives the current density varying with the depth x as[5]

$$J_z = \sigma E_z e^{-x/\delta_s} e^{-ix/\delta_s} \quad \text{amp/m}^2 , \qquad (1)$$

where the normal skin depth, δ_s, is defined as

$$\delta_s = (\rho/\pi f \mu_o)^{1/2} = 504\ (\rho/f)^{1/2} \quad \text{meters} \qquad (2)$$

for ρ in ohm-meters and f in Hz. The resistivity, for a semiconductor whose dominant charge carrier has an effective mass m^* and mean-free time between collisions of T, can be expressed[6] by the product of T and the carrier concentration n as

$$\rho = \frac{m^*}{e^2} \frac{1}{nT} . \qquad (3)$$

Usually T and n are each significant in characterizing the crystal.

It might be noted in passing that this normal skin depth is small in our best metallic conductors even at power line frequencies. For example, Equation 2 indicates, as is found in practice, that $\delta \cong 7$ mm in copper and in aluminum at 60 Hz and at room temperature.

1. Use of Radio Frequencies to Microwaves

Returning to the choice of method to characterize a flat semiconductor crystal by its resistivity in the volume encompased by the depth of $x \cong \delta$ below the surface, we can choose the frequency to use in order to probe the predetermined depth, δ. Likewise, we can choose the frequency to obtain a reasonable resolution of the mapping since the minimum surface area (= resolution element) that can be probed measures approximately one-half wavelength across. In any case, an instrumental measurement of a value for the skin depth at a given frequency will give, by Equation 2, the effective resistivity near the crystal surface, averaged over the area exposed to the radiation.

For conducting crystals, the normal skin effect applies to within a few percent[7] with the mean-free path of the charge carriers equal to one skin depth as given by Equation 2. Values for the normal skin depth are, by Eq. 2:

For resistivity of 10 ohm-cm, δ_s = 16 mm at 100 MHz,

δ_s = 1.6 mm at 10 GHz, and

δ_s = 0.8 mm at 35 GHz.

For resistivity of 0.001 ohm-cm, δ_s = 0.16 mm at 100 MHz, and

δ_s = 0.008 mm at 35 GHz.

Values to 60 GHz are given for silicon in a recent book by H. F. Matare.[8] Comparison to carrier mean-free path, ℓ, can be made by the "free electron" model[6] for our semiconductor crystal by estimating the Fermi velocity, v_F, to be $1(10^7)$ cm/sec for $m^* = m_e$. The expression for mean-free path is

$$\ell = v_F T.$$

Values of $T = m^*\mu_H/e$ depend on the Hall mobility, μ_H. So the values of mean-free path, ℓ, expected for "free" electrons in our semiconductor at room temperature are estimated to range from ℓ = 0.4 micron for $\mu_H = 10^4 cm^2/Volt\ sec$ to ℓ = 0.04 micron for $\mu_H = 10^3 cm^2/Volt\ sec$. Clearly, we expect $\ell << \delta_s$.

Therefore, the classical expression for the skin depth (δ_s by Eq. 2) should be an accurate way of calculating the resistivity of flat semiconductor samples from measurement of skin depth, δ, even at frequencies higher than 35 GHz.

Cyclotron resonance and electron spin resonance can give useful characterization within the skin depth region too. For example, the concentrations of impurities in Ge were recently measured[9] by cyclotron resonance.

2. Use of Optical Radiation

Coupling to a semiconductor at optical frequencies can yield electrical characteristics.[10] For thin semiconductor wafers, standard optical (infrared) measurements of reflection and transmission have been used to map carrier concentration and mobility; the report by Black, et al.[2] indicates precision better than 10% over a wide range of values for GaAs wafers scanned with a 1.5 mm diameter beam on a Perkin Elmer Model 621 recording spectrophotometer.

NASA's needs include the ability to characterize the surface of more massive semiconductor crystals - possibly too thick to obtain infrared transmission values as above. For certain semiconductors, like Si and Ge, edge contacts will serve to obtain a map of photovoltaic (PV) response from a spot of light impinging on the crystal surface, revealing nonuniformity of carrier concentration and/or mobilities. Meaningful PV response has apparently not yet been attained on other semiconductor crystals, such as GaAs. For large band gap semiconductors like SiC and GaAs, the light emitted by electron-hole recombination processes has been used[11,12] to identify the electrically active impurity sites present. Our success at obtaining impurity concentration in volumes of GaAs less than a cubic millimeter is mentioned in the Results Section.

Another class of optical techniques which has promise for electrical characterization involves photo-induced changes. We looked briefly for photo-induced conductivity at room temperature,[13] but our search was inconclusive. Photo-induced microwave conductivity is still a potentially useful technique for mapping high quality semiconductor crystals without contacts.

C. Crystal Selection for this Study

The crystals of semiconductors used in this study of nondestructive techniques for observing electrical characteristics were supplied through the good offices of the NASA Space Sciences Laboratories, MSFC. The emphasis during the earlier portion was on characterizing flat surfaces of GaAs in preparation for the M555 Flight Experiment. The emphasis during the last six months was on small single crystalline flakes of vapor-grown germanium selenide. The comparison of 35 GHz skin depths we observed in GeSe flakes grown[14] on Skylab to GeSe flakes grown at RPI is tabulated below.

D. Purpose

It was, therefore, the general purpose of this contract to demonstrate the sensitivity of one or more noncontacting methods of electrical characterization of single crystals of the semiconductors to be grown on Skylab. Specific goals dealt at first with characterizing surfaces of gallium arsenide slabs and dealt in the last half year with small flakes of germanium selenide single crystals.

Single crystal samples to be studied were supplied through the Space Sciences Lab of NASA/MSFC. The specific approaches that we investigated included microwave skin depth and e-h recombination luminescence. Two microwave techniques were developed to the point of collecting statistical evidence of sensitivity and reproducibility. The GaAs luminescence scanning technique was developed by an interested graduate student J. M. Rowe, largely on his own time.

II. APPROACH TAKEN

A. Noncontacting Techniques Considered

1. RF Resistance by Coil Loading

The eddy currents induced in a semiconductor specimen are a specific but complicated geometric function of shape of coils and semiconductor and of the uniformity of resistivity. An example of successful noncontacting measurements of bulk resistivity by eddy currents at 10 MHz was reported by J. C. Brice and P. Moore in J. Sci. Inst. 38 (1961) on page 307. Mapping could be accomplished with sufficiently small coils but consistent coupling is a difficult mechanical problem.

2. Surface Effects at 9 GHz and 35 GHz

Preference was given to 35 GHz because the area of the mapping resolution element can be smaller by x16. We considered the surface resistance by waveguide termination[15] and by cavity loading, preferring the latter for flats with high resistivity and for the small flakes. We considered the microwave Hall effect. After several tries with biomodal cavities, we became more fully appreciative of the critical need for equivalence in the degenerate modes as called for by A. M. Portis in his Phys. Rev. paper, a truly severe mechanical challenge and, therefore, not suitable for rapid surveying of flat samples.

Cyclotron resonance remains a promising prospect[9] for measuring the lifetime of each type of carrier provided the mapping can be arranged at low temperatures.

Photo-induced changes in microwave conductivity (PC) similarly stands as a promising non-contacting way[13] of mapping several electrical characteristics with a resolution element approaching the size of the minimum light beam. Photo-induced microwave conductivity should be especially useful in semiconductor samples of very high resistivity for which the sensitivity of surface resistance measurements is declining.

3. Optical Means

Fluorescence from electron-hole recombination is frequently a direct indicator of the donor impurity density.[10-12] The literature is literally crowded with publications of such observations for semiconductors at low temperatures. We found little evidence of successful fluorescence at room temperature so we took up that challenge.

Raman scattering from defect modes at the impurities of interest is weak at room temperature being usually not sensitive enough to reveal the impurity concentrations of interest even at very low temperatures.

B. Noncontacting Techniques Used

Each technique for noncontacting electrical characterization of semiconductor surfaces was chosen to demonstrate its reliability for absolute values in a sample sequence representative of the short term needs of NASA's program for space crystallization. Repeated substitution of samples was employed to attain preliminary statistical evidence of reliability.

It should be noted that in any sequential substitution method there are sources of dc noise which can be reduced or eliminated by properly engineered modulation techniques. Therefore, the reliability or signal-to-noise reported here represent conservative values - susceptible of improvement by one or more orders of magnitude with the appropriate engineering.

1. Skin Depth at 35 GHz

Resistivity near a semiconductor surface is related to the skin depth, δ_s, observed at the frequency f by Eq. (2) above. The sensitivity of the measuring circuit to small changes in δ_s depends on the way the semiconductor surface is coupled to the circuit. Two styles of coupling - cavity loading and waveguide termination - were chosen in order to cover a broader range of resistivity values.

a. Cavity loading, especially for small single crystals. The loss introduced into the circuit by a sample of semiconductor surface will be a small fraction of the "no-sample" circuit losses when the product[16] of the surface area times the skin depth δ_s is small. This occurs both for small crystals of normal resistivity and for larger sections of large flat surfaces of high resistivity. Cavity loading is preferred because it raises the strength of the electromagnetic field at the semiconductor surface relative to its strength in most other parts of the detecting circuit and this leads to greater sensitivity to losses in the semiconductor surface than without the cavity.

This section describes: 1.) the microwave circuit which was arranged and calibrated to yield signals reliably corresponding to absolute cavity parameters and 2.) the type of substitutional cavity loading used. Our analyses for converting cavity parameters into values of skin depth of the semiconductor sample are given in the appendices.

1.) The double-arm 35 GHz circuit used. In Fig. 1, the 35 GHz double arm reflectometer is shown schematically with a reflective

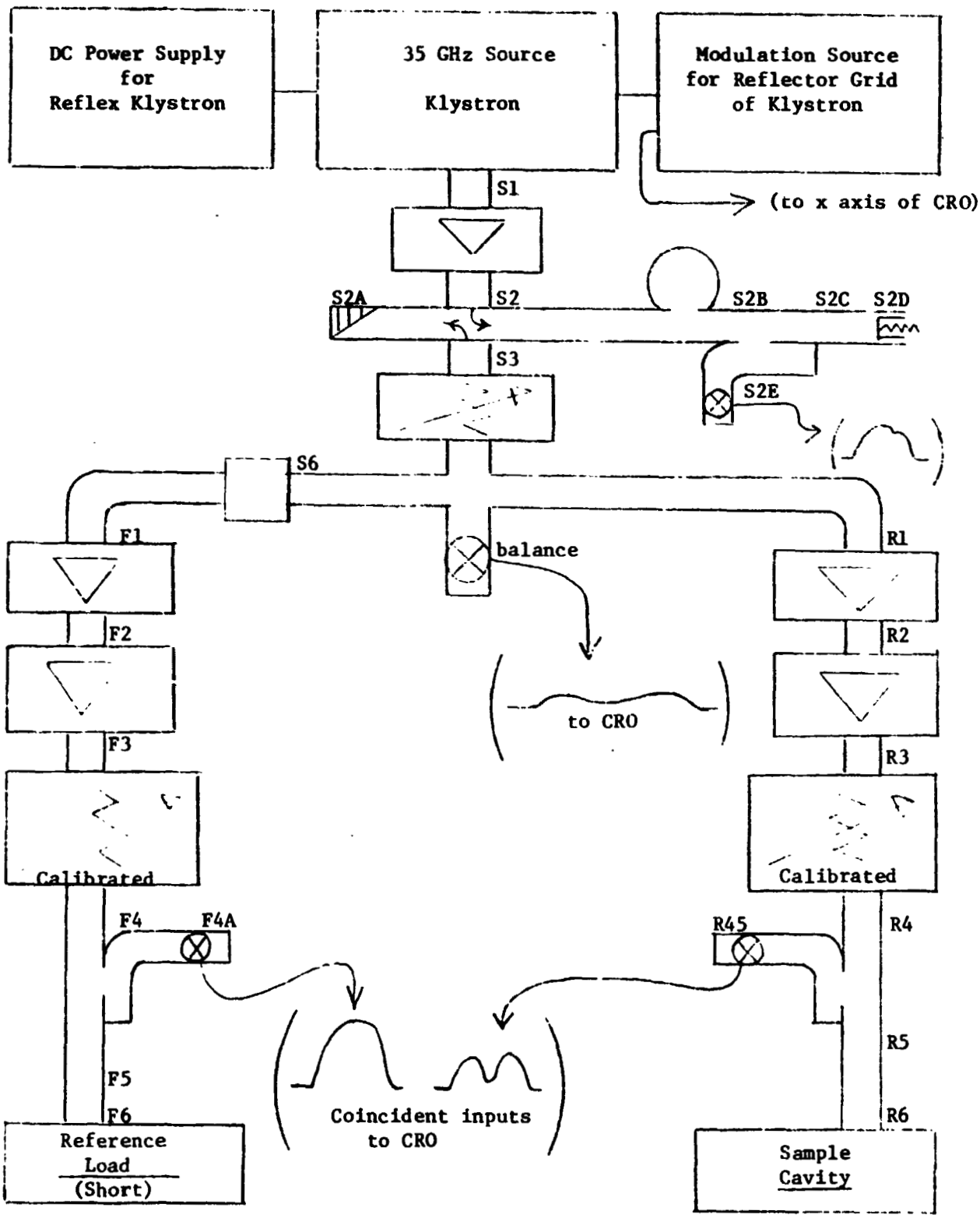

Fig. 1. Schematic of 35 GHz Double-Arm Reflectometer

TABLE 1

COMPONENTS USED IN 35 GHz DEMONSTRATION DOUBLE ARM REFLECTOMETER

Label on Figure 1	Item - Function	Specific Type Mfg. - Model No.
	DC Power Supply	NARDA Model 438
	Modulation Source	NARDA 438
Kylstron	Source of 35 GHz Power	Varian VA-97
S1	Isolator (20 db)	TRG A110-95
S2	Directional Coupler (20 db)	Microline 405A
S2A	Matched Load	Part of S2
S2B	Frequency Meter (Tunable Cavity)	H-P R532A
52C	Directional Coupler (20db)	Microline 429A
52D	Waveguide Short (Adjustable)	
52E	Crystal Holder (Tunable)	Demornay Bonardi
S3	Attenuator (Variable)	Lieco 10V1-26
S4	Mgic Tee (4 arm)	Demornay Bonardi
S5	Crystal Holder (Tunable)	
S6	Slide Screw Tuner (for balancing Tee S4)	Demornay Bonardi DBD 919
Front Arm		
F1	Isolator (20 db)	Uniline by Cascade Res.
F2	Isolator (20 db)	TRG A110-39
F3	Calibrated Attenuator of Rotating Vane	H-P R382A
F4	Directional Coupler (10 db-broad band)	TRG A561-10

Table 1 - (Contd)

Label on Figure 1	Item - Function	Specific Type Mfg. - Model No.
F4A	Tunable Crystal Holder (Containing MA494 crystal selected for having power response (I vs. P_{in}) similar to the crystal in holder R4A)	Microwave Associates Mod. 5130
F5	Waveguide (connection between reference short and front directional coupler)	UAH - usually included a piece of stainless steel waveguide 20 λg long 8.448 $\pm$ .002 inch, having 2.2 db round trip loss.
F6	Reference Load - A low loss, $\lambda g/4$ short arranged by F5 to be the same path length from the front F4 directional coupler as the sample cavity iris is from the rear R4 directional coupler.	UAH - Dwg available.
Rear Arm - Each corresponding item is the same model as in the front arm, except:		
R6	Sample Cavity - usually TE_{015} mode rectangular cavity incorporating: 1. Special sample holder 2. Fixed (but demountable) coupling iris.	UAH - assembled copper pieces, dwgs available.

sample cavity on one arm and a high quality waveguide short on the reference arm. The list of the components used in this circuit is given in Table 1 and points to the identical characteristics of the two arms, including matching the power response of the detecting crystals over the frequency range of some 100 MHz width.

Frequency modulation over one klystron mode presented the two crystal outputs simultaneously on a double input scope. By careful calibration, including frequent substitutions of standard metal samples, the desired cavity reflection coefficient change was determined from the change in the calibrated attenuator R3 required in order to rematch the CRO traces upon each substitution of the sample. The formulae used are given separately in an appendix for the different types of cavity loading.

2.) Types of cavity loading used. Rectangular TE_{01p} mode cavities were constructed of milled sections of copper bolted together with one section carrying a fixed circular iris[17] in a thin (.020 inch) wall and one section mounting the sample. With the minimum milled radius of inside corners at .016 inch, we found it necessary to have the sample cavity at least five half wavelengths (p = 5) long. Greater sensitivity will accrue to sample cavities formed to permit p = 2. The need for the fixed iris is evident in the formulae in the appendices, permitting cavity changes upon substitution to be related solely to the sample. The original and still useful reference on iris deisgn is MIT Rad Lab Report 43-22 by H. A. Bethe.[17]

Loading of the cavity by a semiconductor surface was done in one of two ways: by replacing the end wall or by adding surface in the transverse plane at one-half wavelength from the end wall. Flat GaAs surfaces were held at the end of the rectangular TE_{01p} mode and leakage losses were held to a satisfactorily low level by appropriate choke joints. Clearly an improved design with much lower coupling losses would involve a sample cavity in the shape of a right circular cylinder[4] and the semiconductor flat as its end wall or central portion thereof.

Thin semiconductor (GeSe) flakes whose other two dimensions were under 7 and 3.5 mm, respectively, were suspended between two strips of plastic (sample holder) at one half wavelength up. Fig. 2 indicates the microwave magnetic field pattern in the last two half wavelengths in the TE_{01} mode, outlined by the cavity walls and intercepted by the sample at one-half wavelength up where the microwave magnetic field is parallel to the largest faces of the thin flakes. Our tests indicated no appreciable mode distortion by the thin GeSe flakes used so the observed changes in Q were related to losses on the GeSe surfaces. We assumed these losses were conduction losses within the GeSe and calculated the appropriate skin depths after integrating over the flake area.[16]

b. Waveguide termination. For mapping flat semiconductor surfaces having low resistivity (below about 1 ohm-cm), the simple termination of a waveguide by the sample surface being held across the guide opening will give reasonable sensitivity. One expects, for example, a factor of 4 in standing wave ratio at 35 GHz for a factor of ten in resistivity

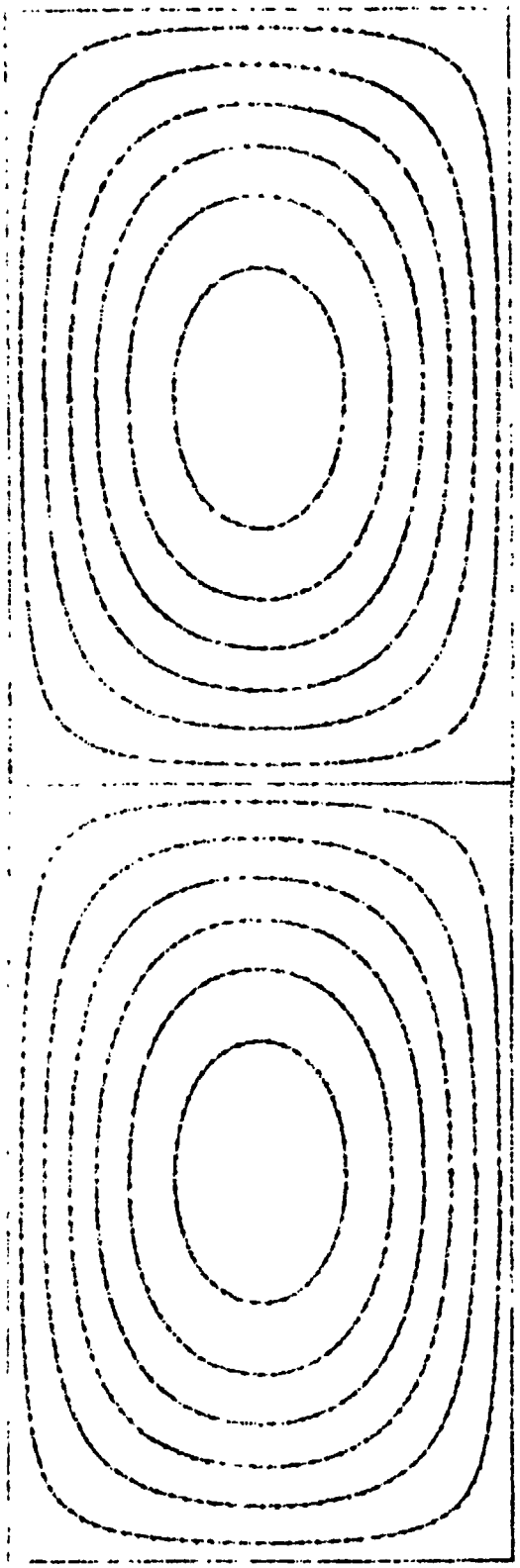

Fig. 2. One wavelength of the pattern of microwave magnetic field in rectangular TE_{01p} mode sample cavity as viewed through a broad face.

Credit: George R. Smith for this accurate representation of the H-pattern and its generation using an HP 9100 Plotter.

according to Lundmayer et al.[15] Again, the effects of leakage on variations in the choke coupling can be effectively eliminated for surfaces flat to within one or two degrees over small sampling areas by using circular guide.

Our preliminary tests confirmed the suitability of choke coupling for mapping GaAs flats with as cut surfaces when held as rectangular waveguide terminations.

2. Fluorescence from Electron-Hole Recombination

The recent surge in the semiconductor market for light-emitting diodes for optical couplers and lasers as well as for displays has placed considerable additional premium on improving semiconductor crystal quality in the category of gallium-aluminum phosphide-arsenide. Of special interest is the spectrum of luminescence and the density of donor sites. Our fluorescence method of surface characterization dealt directly with these two properties of a GaAs surface on a resolution scale of a fraction of a mm. Fluorescence measurements are inherently capable of characterization on a resolution scale of the dimensions of either the carrier mean-free path or the diffraction limit of the optical system used to excite the carriers - whichever is the larger for the sample in question.

The strong market for microwave generation and light modulation in Ga-Al-P-As semiconductors merits more direct measurements of carrier lifetimes than by standard fluorescence. We suggest optically-pumped cyclotron resonance should do well.

Our approach was to use the photoluminescence reported[10,12] for gallium arsenide crystals at low temperatures, where the different kinds of donor centers can be resolved in the emission spectra, in interpreting the room temperature luminescence. We pumped a spot about 0.5 mm diameter on a GaAs surface with a laser beam, delivering some 20 milliwatts at 632.8 nm, and collected the emission over a solid angle of approximately 0.3 steradians not including the angle of specular reflection. After passing through a double monochromator at low resolution (1 mm slits), a narrow band of the emitted light is collected on a red sensitive photomultiplier tube (C3893) and the output displayed on a chart recorder as the monochromator wavelength is scanned from 8200 Å to 8800 Å in about 10 minutes.

The principal features of a chart record of the room temperature fluorescence from a single spot on GaAs are: the total intensity, the wavelength of the maximum intensity and the widths of the low energy tail and of the high energy side. A typical spectrum from GaAs is displayed in Fig. 3. Mapping is done effectively by repositioning the GaAs surface for each spot of interest, with micrometer drives.

Credit goes to Mr. James M. Rowe for arranging, calibrating and tuning up the apparatus to the state where we could scan a set of spots and then get reproducibility in total intensity to within ten percent. The wavelength for the peak indicates the kind of e-h recombination center active (usually a donor site). When the tails on either side are narrow, the total intensity is related directly to the number of these donor centers being excited by the pump light. With the focus and power of the pump light held constant, the total emitted intensity is proportional to the local concentration of donors.

Identification of the type of donor site by correlation with the value of the wavelength at the peak of each spectrum will require correction of the PMT output to one proportional to the number of photons collected. J. M. Rowe used a standard lamp to calibrate the PMT output and with the aid of Karla Dalton prepared an effective computer program for carrying out this correction procedure. The program's flow chart is given in the last appendix. The output of the program in its present form is automatic graphing of: the input spectral data, the corrected PMT output vs. wavelength, and the corrected PMT output vs. energy of the emitted photons. Examples of these automatic graphs for the emission spectrum of one spot on a GaAs as-cut surface at room temperature are displayed in Figures 3, 4 and 5.

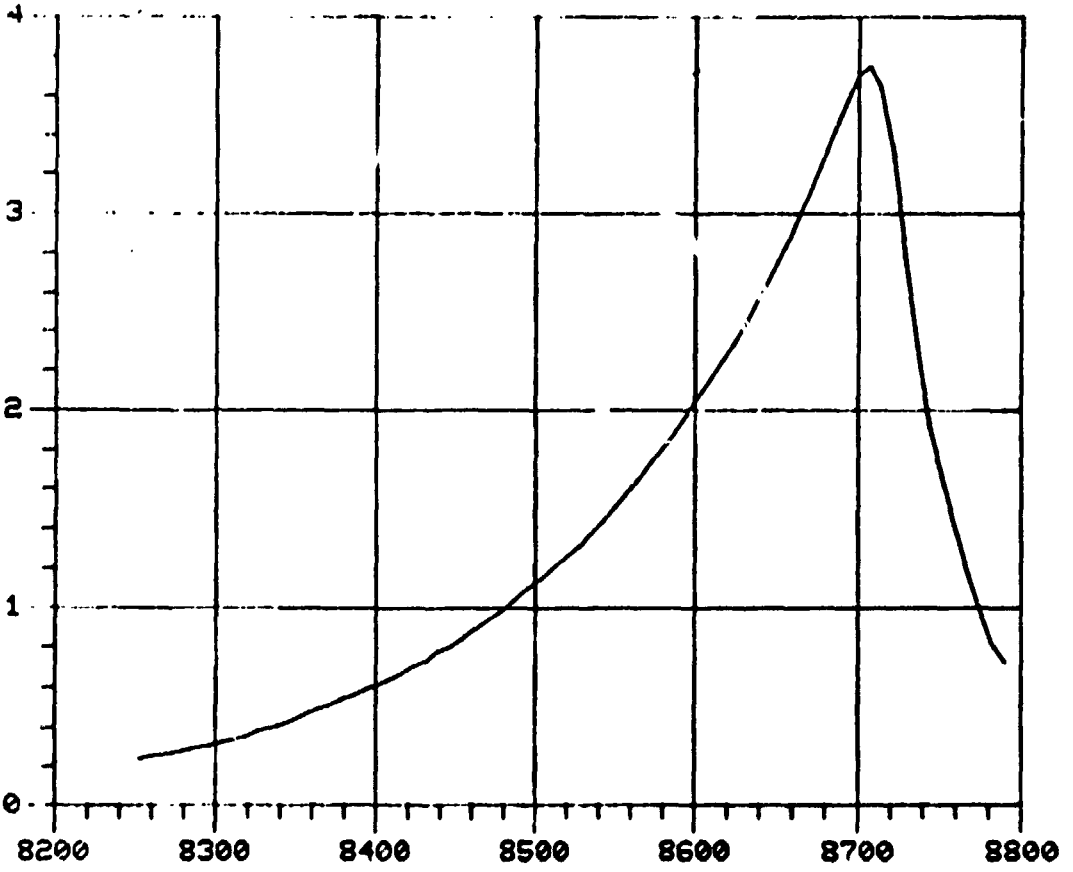

CORRECTED PMT OUTPUT, AMPLITUDE VS WAVELENGTH

736-1120 C DATA SOURCE

Fig. 3. Photoluminescence Observed from GaAs.

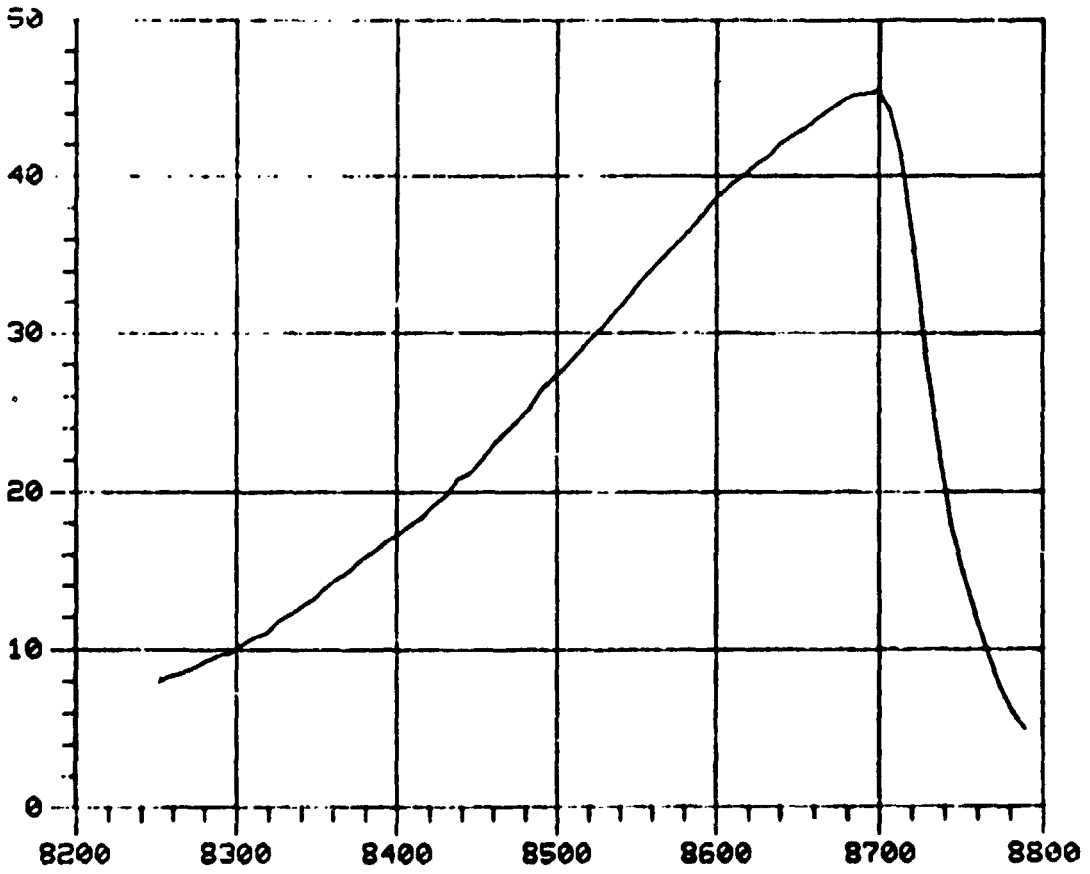

PMT OUTPUT, AMPLITUDE VS WAVELENGTH

736/120 C DATA SOURCE

Fig. 4. PL from GaAs.

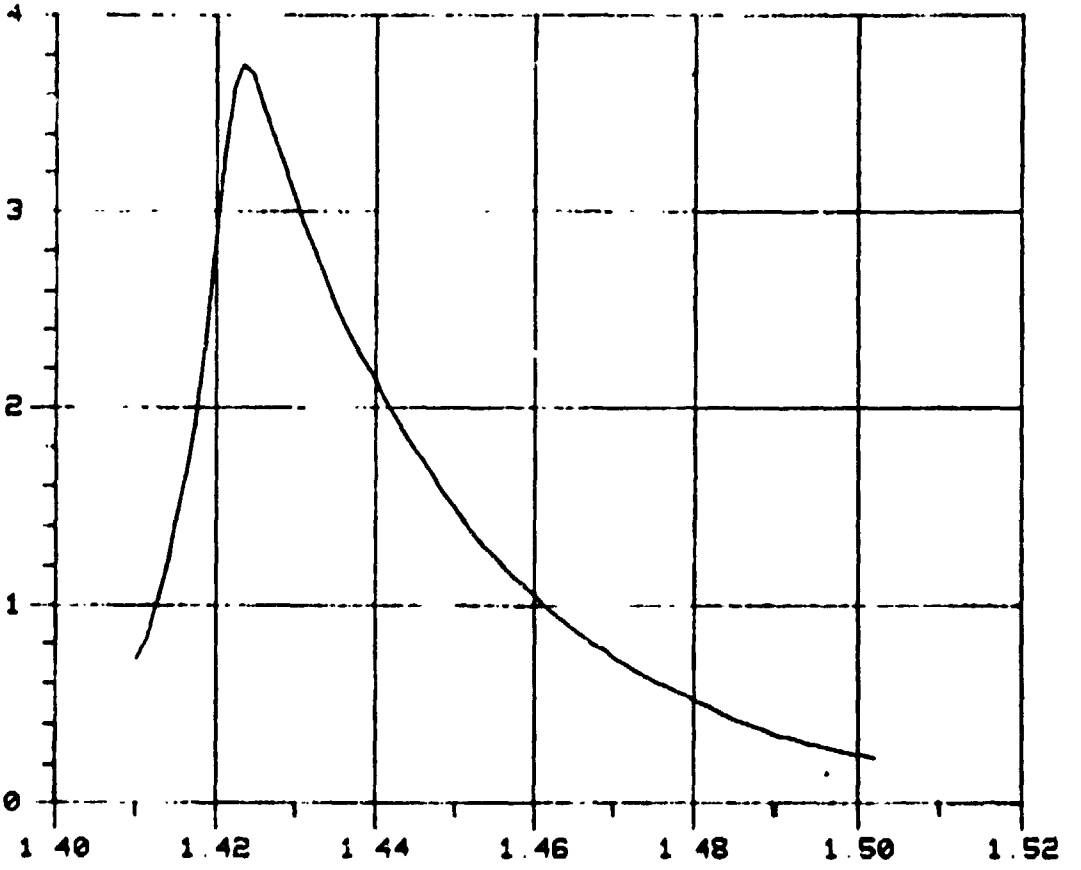

CORRECTED PMT OUTPUT, AMPLITUDE VS ENERGY(EV)

73G1120 (2) DATA SOURCE

Fig. 5. PL from GaAs

III. RESULTS - DEMONSTRATION OF SENSITIVITY OF NONCONTACTING TECHNIQUES

In direct assistance to the NASA space processing program, this study has developed three noncontacting techniques into successful laboratory procedures for the nondestructive electrical characterization of single crystal semiconducting surfaces. Time permitted only preliminary measurements with each of the three procedures, but an indication of their sensitivity is given in the precision stated below for the measured characteristics. Values obtained for the skin depth at 35 GHz and 300 °K in selected GaAs surfaces are listed, following a description of the skin effect found in a few of the GeSe flakes grown on Skylab missions.

A. Skin Depths in GeSe Flakes at 35 GHz

The high quality single crystal flakes produced by vapor transport in ampules in Skylab's multipurpose furnace were thin platelets a few square millimeters in area. We developed the procedure described above for loading a room temperature 35 GHz copper cavity with one GeSe flake at a time so that the cavity reflections could be interpreted to yield the ratio of the skin depth averaged over each flake to the skin depth of the copper walls of the cavity. A precision measurement of cavity Q would then yield a precise value of the average δ in each flake.

In our preliminary laboratory operation, we obtained introductory information on several specific questions about the use of 35 GHz radiation to characterize small semiconducting crystals. First, our procedures are capable of characterizing without damage the skin depth of each of a large number of crystals per day. Secondly, centering of the sample was judged visually and remained one of the principal sources of fluctuation in our

observed values. Except for more difficult sample handling, the same cavity loading procedures work at liquid nitrogen temperature with the expectation of even better sensitivity. Some care must be exercised in the choice of materials for holding the sample flakes in place within the copper cavity, but polyethylene film appears to serve well at our present sensitivity. It should also be noted that the surface currents induced in the flat platelet when properly mounted in cavity are all in one direction, the same on both sides of the platelet, permitting thereby a search for anisotropy in the resistivity of each semiconductor crystal.

One operational aspect was tested - namely the skill level required for carrying out the cavity loading observations on GeSe at 35 GHz. After the selected GeSe flakes had been measured by a highly experienced operator (#1) to be certain that the loading procedure functioned satisfactorily, in the reflection cavity (A), verbal instructions were given to a new technician (operator 2) who had experience with ham radio but none with microwaves. Operator 2 then surveyed the same samples in cavity A and again in a modified cavity (B) in which the end of the cavity had been modified to permit transmission measurements.

The room temperature results are summarized in Table 2. The relative Q factors (Q_s) of each sample to that (Q_w) of the cavity walls are listed as an aid to later evaluation of this cavity loading technique. Pertinent details are listed in the appendices.

Inspection of Table 2 shows how the GeSe skin depths vary between these five crystals by a factor of 6. The corresponding range of equivalent

TABLE 2

RELATIVE Q AND SKIN DEPTHS FOR GeSe FLAKES
AT 35 GHz AND ROOM TEMPERATURE

Crystal		Q_{wall}/Q_{sample}					δ_s
Label	Total Area mm^2	Combinations Used●● A,1	A,2	B,2	Mean Value Q_w/Q_s	δ_s/δ_{cu}	micron●
3B-FS	1.86	0.119 ± .015 from 3*	0.134 ± .013 from 2*	0.159 ± .015 from 2*	0.137 ± .014	16.2 ± 1.6	5.7
3B-F6	0.96	0.018 ± .003 from 6*	0.014 ± .004 from 2*	0.015 ± .005 from 2*	0.016 ± .004	3.7 ± 0.9	1.3
3A-F1	1.11	- tried 2*	- tried 2*	0.015 ± .005 from 2*	0.015 ± .005	2.7 ± 0.9	0.9
3A-F2	0.89	0.016 ± .005 from 4	0.038** ± .008 from 2*	0.020 ± .005 from 2*	0.025 ± .010	6.0 ± 2.4	2.1
RPI-A (H1)	6.5	0.150 ± .005 from 2*	0.149 ± .005 from 2*	0.139 ± .02 from 1*	0.149 ± .005	2.9 ± 0.1	1.03

* Number of independent substitutions of sample into cavity.

** First set for operator 2

● Calculated with δ_{cu} = 0.15 micron

●● Combinations used were Cavity A by operator 1, Cavity A by operator 2, and Cavity B by operator 2.

bulk resistivities is a factor of 36. The uncertainties observed would have been reduced - probably to $\pm$ .003 in Q_w/Q_s - by using ten or so independent substitutions of the sample during each run.

The data represented in Table 2 also confirm the soundness of our theoretical analysis in regard to sample configuration. The absolute values of the skin depth, δ_s, listed in the last column of Table 2 confirm the validity of the flakes being thick compared to their own skin depth so that the power loss in a flake is the same kind of product[16] of surface integrals of H_T^2 as for the copper walls. Secondly, the flakes were thin enough to permit using the undistorted mode values for H_T across the sample.

A final note about sensitivity of this cavity loading substitution procedure is that when a flake of ultra high purity aluminum foil was the substituted load, the minimum detectable area was about 3 mm^2 of Al. As the resistivity of the semiconductor flake is increased, our cavity loading signals become larger, indicating the capability of characterizing smaller flakes or of obtaining more precision. For example, the observed standard deviations listed in Table 2 give: $\pm$ 3% for a 7/2 mm^2 flake having δ_s = 1 and $\pm$ 10% for a 1.9/2 mm^2 flake having δ_s = 6 micron.

B. Skin Depths in GaAs Flats at 35 GHz

High quality boules of GaAs grown by M. Rubinstein of Westinghouse Research and Development Center in preparation for the M555 Experiment on Skylab had been sliced for characterization. Several cut faces, termed flats, were mapped for skin depth at 35 GHz using a resolution element of 4 x 7 mm as the rectangular TE_{01p} cavity end wall in the procedure mentioned

above. Cavity reflections were interpreted in accord with the analysis outlined in the appendices in terms of the skin depth δ_s in the GaAs. Some of the average values found for δ_s are listed in Table 3, taking $\delta_{Cu} \sim 0.35$ micron.

TABLE 3

CLASSICAL SKIN DEPTH

Sample	Cs^1(p=13) δ_s(mm)	Cs^2(p=7) δ_s(mm)
W-2	$(1.178 \pm 1.2) \times 10^{-2}$	(--)*
W-3	$(2.053 \pm 2.66) \times 10^{-2}$	$(1.014 \pm 0.3) \times 10^{-2}$
E-2	$(2.423 \pm 2.07) \times 10^{-2}$	$(2.056 \pm 0.6) \times 10^{-2}$

*A value for δ_s was not obtainable from the data.

The uncertainty in the measured values was much larger than the limiting uncertainty due solely to the ability to read the equipment accurately. Evidently the variations in resistivity between the areas being sampled are comparable to but not much larger than the variations in coupling as an end wall in one positioning of the sample. Precision improvement of almost one order of magnitude is expected in the same procedure when the shape of the sample cavity is a right circular cylinder and the resolution element of the semiconductor flat is the circular end wall or a concentric circular portion.

The actual values obtained, however, from the two cavities, Cs^1 and Cs^2, for the classical skin depth of the samples, are in good agreement. Clearly the shorter cavity produces higher precision as expected. Again, when

machining or etching techniques are used that permit sharper inside corners (than r = 0.016 inches), then p = 2 cavities can be used and precision will be improved over the p = 7 cavity.

C. Mapping of GaAs Single Crystals by Fluorescence

Photo-induced luminescence of the electron-hole recombination radiation has been observed by J. M. Rowe from cut faces (flats) of several high quality GaAs crystals. The technique outlined above permits mapping by repositioning the flat in the plane of its irradiated face by micrometer drives. A spectrum is scanned for each position of the laser beam spot. Fig. 3 shows, with the aid of automatic graphing on the UNIVAC 1108 computer, the typical spectrum emitted from a spot on the face of a crystal doped with $\sim 10^{17}$ donors/cm^3. The total intensity (proportional to the donor concentration[10]) was found to be reproducible to $\pm$ 10% for 10 minute spectral scans of the same spot location and relocations. Observed variations across a sample were occasionally 50% and were, therefore, attributable to donor concentration variations, but no direct corroboration of the same surface profile was available at the time of the fluorescence scans. The automatic correction of PMT output via standard lamp calibration is discussed in an appendix and the corrected results plotted in Fig. 4 and 5 of the spectrum of Fig. 3.

Uniformity of surface roughness probably represents the ultimate limit to the precision of this high resolution method of characterizing the donor concentration. Changes in the type of donor will shift the peak of the spectrum. For example, nitrogen donors are a few millielectron volts below the band edge at Eg ~ 1.43 eV. No attempt was made to correlate peak position

with active donor types, but it is clear[12] that lower temperatures permit complete resolution of each type of donor traps.

IV. SUMMARY AND PROGNOSIS

The results of this study of nondestructive methods of electrical characterization of the higher quality single crystals of semiconductor grown in the microgravity of space environment include both the demonstration of successful methods - two microwave and one optical - and the measurement of the resistivity of a few of the small GeSe crystals grown by vapor deposition on Skylab flights. The observed sensitivity of the two microwave methods - one for mapping large flat semiconductor surfaces and one for observing the whole surface of small thin flat crystals - is reported for a limited range of resistivity. The relative skin depth values for the GeSe flakes studied by a sample substitution procedure were found to have standard deviations around 10% for rather small crystals. The absolute skin depth values could readily have had the same precision if we had made the frequency measurements which lead to the absolute Q_L values.

Our prognosis is optimistic, namely that these room temperature microwave techniques can be carried out nondestructively using light weight apparatus with adequate precision for measuring uniformity of resistivity of high quality semiconductor surfaces. Furthermore, related noncontacting techniques such as cyclotron resonance and photoinduced microwave conductivity show promise of being useful sources of electrical characteristics of the high quality semiconductors to be grown in space.

The observed reproducibility of the fluorescence of room temperature GaAs under irradiation at 632.8 nm of some 10% in donor density for our slow scan technique also shows promise for NASA applications. Actually, with the large expansion in the light emitting diode production in the

past several years, the LED manufacturers very likely have a similar optical scanning technique in regular use by now.

V. REFERENCES

1. c.f., C. Richard and M. Dugue, "Photoconductivity Associated with Free Excitons in GaAs," Phys. Stat. Sol. (6) 50, 263-269 (1972) and references therein.

2. J. F. Black, E. Lanning, and S. Perkowitz, Infrared Physics 10, 125-139 (1970).

3. Consult David P. Nicolas, EC43, MSFC/NASA for the capabilities of nondestructive examination by X-ray flourescence on his scanning electron microscope.

4. An extended discussion of the skin effect is given by A. F. Harvey in Microwave Engineering, McGraw-Hill Book Co., New York, 1965, p. 256 ff.

5. American Institute of Physics Handbook, D. E. Gray, Ed., McGraw-Hill Book Co., New York, 1957, p. 5-85.

6. C. Kittel, Introduction to Solid State Physics, 4th Ed., J. Wiley and Sons, Inc., New York, 1971, p. 258.

7. AIP Handbook, 1957 Ed., p. 5-200.

8. H. F. Matare, Defect Electronics in Semiconductors, Wiley Interscience, New York, 1971, p. 570.

9. L. E. Blagosklonskaya, E. M. Gersheuzon and Y. P. Lady Zhinskii, "Determination of the Impurity Concentration in Germanium by Cyclotron Resonance," in Soviet Physics - Semiconductors 4 # 6, 1007 (1970).

10. An excellent review of photoluminescence from semiconductors is presented by H. B. Bebb and E. W. Williams in Chapter 4 (Theory of Photoluminescence) and Chapter 5 (Photoluminescence in GaAs) in Vol. 8 of the book series Semiconductors and Semimetals, R. K. Willardson and A. C. Beer, Ed's., Academic Press, New York, 1972.

11. For SiC, c.f., W. J. Choyke and L. Patrick, Phys. Rev. B5, 3253 (1972).

12. For GaAs, c.f. E. W. Williams and C. T. Elliott, Brit. J. App. Phys. (J. Phys. D) Ser. 2, Vol. 2, 1657-1665 (1969).

13. Photoconductivity was reported in ref. 1 for GaAs only at low temperatures.

14. H. Weidemeyer, P. I., Contract NAS8-26146.

15. J. Lindmayer and M. Kutsko, Solid-State Electronics, Pergamon Press, N. Y., 1963, Vol. 6, pp. 377-381.

16. The appropriate integrals are given, for example, by A. F. Harvey in equation 5.2 of ref. 4.

17. c.f. H. A. Bethe, "Lumped Constants for Small Irises," MIT Radiation Laboratory Report 43-22, dated March 24, 1943. Unclassified. 40 pages.

APPENDIX A

ASSUMPTIONS FOR EQUATIONS IN APPENDICES B AND C

If all of the microwave energy is stored in the rectangular cavity in only one TE_{01p} resonant mode, it is possible to find a point, z_o, such that the electric field is 0, independent of the x and y positions and time. Thus, we can insert a very thin conducting sample and a sample holder, made of a dielectric, at that point, with its thin dimension parallel to the z-axis without changing the electric field. If $\mu_s = \mu_H = \mu_o$, where μ_s is the permeability of the sample and μ_H is the permeability of the holder, then we do not change the magnetic field and thus the energy stored in the empty cavity is the same as that of the cavity with sample holder with or without the sample.

If the electric and magnetic fields are not altered within the cavity by the addition of the sample holder and sample, then the intrinsic impedance of the cavity has not changed. Thus, the energy radiated out the coupling iris, back down the waveguide should not change. This means that, for cases (A) through (C) the value of $\left(\frac{1}{Q_{c,1}}\right)$ should be the same. Similarly, if, by adding the sample and sample holder to the empty cavity, we do not change the current density in the cavity walls, then the ohmic losses due to the walls is the same in cases (A) through (C). This can be done, for example, by making the sample holder out of a lossless dielectric so that the conducting sample is isolated from the walls of the cavity. A problem can arise, however, in the manner in which the sample holder and sample are inserted into the cavity. In this particular process, a slot was cut into the side of the cavity. This means that some power was

radiated out of the cavity. This loss is usually neglected in the total loss of power due to the walls of the cavity. We assume that adding the slot did not change the electric and magnetic field configuration in the cavity, and, as we are in a TE_{01p} mode, this means that at Z_o, where the slot was made, the tangential electric and tangential magnetic fields are both zero. Thus the amount of energy radiated out of the cavity is only a small part of the total wall losses. Thus, altering this amount of radiated energy, such as is caused by inserting the dielectric sample holder into the slot, does not significantly alter the total energy loss due to the walls of the cavity. Hence the value of Q_W does not change for cases (A) through (C). A similar argument shows that the value of Q_W is also a constant for cases (D) through (F).

If we assume that the addition of the second coupling iris does not change the resonant mode electric and magnetic field of the single-line cavity-coupling system, then $\left(Q_W\right)$ does not change from case (A) through (F) as the total energy stored will be the same, and the change in the energy lost due to the walls is not greatly changed by the loss of the surface area, due to the second coupling iris, from $\int_s H_T^2 ds$, which is proportional to the ohmic energy loss per cycle due to the walls of the cavity,[1] where H_T is the amplitude of the magnetic field tangent to the walls of the cavity and the integral is taken over the total surface of cavity walls. The assumption that the addition of the second coupling iris does not change the resonant mode is justified in the equipment and cavities used, by the fact that the resonant frequency shifted by less than 0.1% from the single-line cavity-coupling system to the two-line cavity-coupling system.

---

(1) See E. U. Condon, Rev. Mod. Phys. 14, P-341 (1942).

Finally, if the addition of a second coupling iris does not change the electric and magnetic fields in the cavity, then the value of $Q_{c,\,1}$ is the same in cases (A) through (C) and cases (D) through (F). Thus, the values of Q_W, $Q_{c,\,1}$, Q_s, and Q_H are the same for cases (A) through (F). Hence, equation (18) is justified. It also means that the values of $\beta_{1,\,MT}$ and $\beta_{2,\,MT}$ are the same in both the single-line and two-line cavity-coupling system, so that we can measure both values by using the single-line cavity-coupling system and use these values in an equation that is true for a two-line cavity-coupling system. Thus we can obtain a justifiable value for Q_s using equations (19), (20), and (17) or (17A).

If we still assume that all the microwave energy of the rectangular cavity is stored in only one TE_{01P} mode and that the electric and magnetic fields in this mode are the same for the coupled cavity as for the uncoupled cavity, then the total energy stored in the empty cavity is $\frac{1}{2}\int_v \mu_0 H^2\,dv$ where H is the magnitude of the magnetic field and the integral is taken over the total volume of the cavity.[2] If we insert our sample and sample holder in the cavity at the point Z such that the electric field is zero, then the energy stored in the cavity with the sample and sample holder is the same as the empty cavity.

As the sample is conducting, it will create an ohmic power loss that will increase the energy loss per cycle in the cavity. The energy loss per cycle in the sample is given by $\frac{\delta_s \pi \mu_s}{2}\int_s H_T^2 ds$ where δ_s is the skin depth of the sample and H_T is the magnitude of the magnetic field tangent to the surface of the sample A and the integral is taken over the total surface of the sample.

2. See Fig. 2 of this report for the shape of the H pattern.

$$\text{As } Q_s = \frac{2\pi(\text{Energy Stored in the Cavity})}{(\text{Energy Lost in the sample in one cycle})}$$

and we have already assumed $\mu_s = \mu_0$ we get,

$$Q_s = \frac{2\int_v H^2 d}{\delta_s \int_s H_T \, ds} \tag{27}$$

Using the solutions for the electric and magnetic fields in the TE_{01p} mode [4] and assuming that the sample is a rectangular parallelepiped, we can perform the volume and surface integrals above, remembering that the sample is at z_o, we get,

$$Q_s = \frac{\pi AC[B^2p^2 + C^2]}{4\delta_s B^2 p^2 (\Delta x)\left[\frac{\pi}{2B}\Delta y - \frac{1}{4}\sin\left(\frac{2\pi}{B}y_2\right) + \frac{1}{4}\sin\left(\frac{2\pi}{B}\right)y_1\right]} \tag{28}$$

Where A is the length of the cavity along the x-axis, B is the length along the y-axis, C is the length along the z-axis, Δx is the length of the sample along the y-axis Δy is its length along the y-axis and y_1 and y_2 are the y positions of the sample in the cavity. This result also assumes that Δz of the sample is so small that we can ignore the surface integral over those portions of the surface of the sample that involve Δz. This is justified in all the GeSe flakes measured.

Other shapes will produce other solutions, however, most shapes can be approximated by a rectangular parallelepiped or a sum of such shapes, in which case, the above equation will still hold. Otherwise, other

4. See Technique of Microwave Measurements, Vol II, edited by C. G. Montgomery, P. 295, McGraw-Hill (1947).

coordinate systems and techniques of integration will have to be used. Also, note that the factor of 4 appears in equation (28), rather than a factor of 2, to account for the loss in both sides of the sample, so that, if a sum of rectangular parallelepipeds is to be used as the approximation, this factor can be changed to 2 and the sum carried over both sides independently.

Finally, if we again have a rectangular parallelepiped in which we can ignore the Δz terms and further, that Δy is so small that $\sin^2\left(\frac{\pi}{B}\left(y_1 + \frac{\Delta y}{2}\right)\right) = \sin^2\left(\frac{\pi}{B} y_1\right)$, then we arrive at a good approximation for Q_s by assuming that H^2_T is a constant over the total surface area of the sample; that is

$$Q_s = \frac{AC[B^2p^2 + C^2]}{4\,\delta_s\, Bp^2\, \sin^2\left(\frac{\pi}{B}\left(y_1 + \frac{\Delta y}{2}\right)\right)\Delta x\, \Delta y} \qquad (29)$$

The basic assumption in the choke joint cavity system is that the resonant electric and magnetic fields are the same in all four types of cavities. The same reasoning applies in these sets of cavities in transferring from the single line cavity-coupling system (cavities X, Y, and Z) to the two-line cavity-coupling system (cavity T). Any difference in microwave energy losses, due to the choke joint, between the Z cavity and the X cavity is taken into account by the $Q_{R,\,C,\,H}$ term. Finally, the same reasoning is used in calculating the classical skin depth, δ_s, of the sample from $Q_{W,s}$, as was used in the proceeding cavity system, keeping in mind that now the sample makes up one complete end wall of the cavity.

APPENDIX B

BASIS FOR LOSS CALCULATIONS FOR Cu TE_{01p} RECTANGULAR CAVITIES FOR f LARGE ENOUGH TC SUSTAIN NORMAL MODE CONFIGURATIONS

Terms for Single Line Cavity-Coupling System:

P = $2C/\lambda g$

c = Cavity dimension along z axis

λ_g = Wave length in the cavity at resonance

Q = 2π (energy stored/energy dissipated per cycle)

$Q_{L,MT}$ = Loaded Q of empty cavity

$Q_{L,O}$ = Loaded Q of cavity with sample holder but without sample

$Q_{L,s}$ = Loaded Q of cavity with sample holder containing sample

Q_W = Q of Cu walls of cavity

$Q_{c,1}$ = Q of 1st coupling iris

Q_H = Q of sample holder

Q_s = Q of sample

$Q_{u,O}$ = Q of Cu walls and sample holder

$Q_{u,s}$ = Q of walls, sample holder and sample

β = Geometrical coupling parameter which is a constant for a given iris and cavity mode. Each value of β is obtained from a measured reflected power ratio Γ.

Γ = Power ratio (Power reflected/Power incident at plane of cavity iris)

$\beta_{1,O}$ = Coupling parameter of 1st coupling iris with empty sample holder

$\beta_{1,s}$ = Coupling parameter of 1st coupling iris with sample

$\beta_{1,MT}$ = Coupling parameter of 1st coupling iris with empty cavity

Terms for Two-Line Cavity Coupling System:

$Q_{L,MT,T}$ = Loaded Q of empty transmission cavity

$Q_{L,O,T}$ = Loaded Q of cavity with empty sample holder

$Q_{L,s,T}$ = Loaded Q of cavity with sample holder containing sample

$Q_{c,\ 2}$ = Q of 2nd coupling iris

Q_s = Q of sample

Q_H = Q of sample holder

$Q_{u,O,T}$ = Q of Cu walls and sample holder

$Q_{u,O,s}$ = Q of walls, sample holder and sample

$Q_{c,2}$ = Q of 2nd coupling iris

$\beta_{2,MT}$ = Coupling parameter of 2nd coupling iris with empty cavity

$\beta_{2,O}$ = Coupling parameter of 2nd coupling iris with empty sample holder

$\beta_{2,s}$ = Coupling parameter of 2nd coupling iris with sample holder

f_o = Resonant frequency of empty cavity

$\Delta f(3db)$ = Width of power resonance curve at half-peak values

The following equations are applicable when the loss mechanisms are independent and the microwave energy is stored in only one mode.

Basic Equations for Single-Line Cavity Coupling System:

A. For the Empty Cavity

1. $$\frac{1}{Q_{L,MT}} = \frac{1}{Q_{c,1}} + \frac{1}{Q_W}$$

2. $$\beta_{1,MT} = \frac{Q_W}{Q_{c,1}}$$

B. For Cavity with Empty Sample Holder

3. $$\frac{1}{Q_{L,O}} = \frac{1}{Q_{c,1}} + \frac{1}{Q_W} + \frac{1}{Q_H}$$

4. $$\frac{1}{Q_{u,O}} = \frac{1}{Q_W} + \frac{1}{Q_H}$$

5. $$\beta_{1,O} = \frac{Q_{u,O}}{Q_{c,1}}$$

C. For Cavity with Sample Holder and Sample

6. $$\frac{1}{Q_{L,s}} = \frac{1}{Q_{c,1}} + \frac{1}{Q_W} + \frac{1}{Q_H} + \frac{1}{Q_s}$$

7. $$\frac{1}{Q_{u,s}} = \frac{1}{Q_W} + \frac{1}{Q_H} + \frac{1}{Q_s}$$

8. $$\beta_{1,s} = \frac{Q_{u,s}}{Q_{c,1}}$$

Basic Equations for Single-Line Cavity Coupling System (contd)

For the Empty Cavity

$$9.\quad \frac{1}{Q_{L,MT,T}} = \frac{1}{Q_{c,1}} + \frac{1}{Q_W} + \frac{1}{Q_{c,2}}$$

$$10.\quad \beta_{2,MT} = \frac{Q_W}{Q_{c,2}}$$

E. For cavity with empty sample holder

$$11.\quad Q_{L,O,T} = \frac{1}{Q_{c,1}} + \frac{1}{Q_W} + \frac{1}{Q_{c,2}} + \frac{1}{Q_H}$$

$$12.\quad \frac{1}{Q_{u,O,T}} = \frac{1}{Q_W} + \frac{1}{Q_H}$$

$$13.\quad \beta_{2,O} = \frac{Q_{u,O,T}}{Q_{c,2}}$$

F. For cavity with sample

$$14.\quad \frac{1}{Q_{L,s,T}} = \frac{1}{Q_{c,1}} + \frac{1}{Q_W} + \frac{1}{Q_H} + \frac{1}{Q_s} + \frac{1}{Q_{c,2}}$$

$$15.\quad \frac{1}{Q_{u,s,T}} = \frac{1}{Q_W} + \frac{1}{Q_H} + \frac{1}{Q_s}$$

$$16.\quad \beta_{2,s} = \frac{Q_{u,s,T}}{Q_{c,2}}$$

G. Equations for calculating β

$$17.\quad \beta = \frac{1-\Gamma^{\frac{1}{2}}}{1+\Gamma^{\frac{1}{2}}} \quad \text{for } \beta < 1$$

or

$$17A.\quad \beta = \frac{1+\Gamma^{\frac{1}{2}}}{1-\Gamma^{\frac{1}{2}}} \quad \text{for } \beta > 1$$

β can be chosen to be overcoupled (Eq. 17A) (or undercoupled (Eq. 17)) by convenience of machining and detector sensitivity.

β calculated using equation 17 or 17A is the β of the single-line cavity coupling system. However, as we do not change the normal mode nor the shape of the iris, it, therefore, has the same value as in the two-line cavity coupling system.

The fact that the coupling parameter, β, for each case can be calculated from experimental data leads to several important results. First, by using equations (1) through (8), we can relate the sample losses to the cavity wall losses by equation

$$\frac{Q_W}{Q_s} = \frac{\beta_{,MT}\left(\beta_{1,0} - \beta_s\right)}{\left(\beta_{1,0}\right)\left(\beta_{2,MT}\right)} \tag{18}$$

As all the values on the right can be calculated from experimental measuresments, a value can thus be assigned to $\frac{Q_W}{Q_s}$. From this, a comparison of the Q_s values of different samples can be made in a given cavity, provided the value of Q_W does not change. Experimental confirmation that Q_W had not changed was obtained by finding the value of $\beta_{1,MT}(= Q_W/Q_{c,1})$ [Eq. 2]) to be the same to within $\pm$0.4% each time the empty cavity was measured.

Secondly, using equations (2) and (10) we can replace the Q values in Equation (9) with β values to get equation

$$\frac{1}{Q_{L,MT,T}} = \frac{1}{Q_W}\left(\beta_{1,MT} + 1 + \beta_{2,MT}\right) \tag{19}$$

As we can calculate a value for $(\beta_{1,MT} + 1 + \beta_{2,MT})$, we can thus get a value of Q_W from a known value of $Q_{L,MT,T}$. Finally, we measure the value of $Q_{L,MT,T}$ experimentally by using equation

$$1/Q_{L,MT,T} = \Delta f(3db)/f_o \tag{20}$$

We can arrive at a value of Q_W that is

$$Q_W = \frac{f_o}{\Delta f(3db)} \left(\beta_{1,MT} + 1 + \beta_{2,MT} \right) \tag{21}$$

$$= Q_{L,MT,T}\left(\beta_{1,MT} + 1 + \beta_{2,MT}\right).$$

Thus, using Equations (18) and (21), we arrive at an equation for Q_s,

$$Q_s = \frac{f_o\left(\beta_{1,MT} + 1 + \beta_{2,MT} \right)\left(\beta_{1,0}\right)\left(\beta_{1,s}\right)}{\Delta f(3db)\left(\beta_{1,MT}\right)\left(\beta_{1,0} - \beta_{1,s}\right)} \tag{22}$$

dependent totally on measurable quantities.

By using the previously mentioned equations, we can also make measurements on the uncertainty of the quantities Q_W/Q_s and Q_s

First, by using Equation (15) we find the uncertainty $\Delta\left(Q_W/Q_s\right)$ is given by

$$\Delta\left(Q_W/Q_s\right) = \left[\frac{\left(\beta_{1,0} - \beta_{1,s}\right)}{\left(\beta_{1,0}\right)\left(\beta_{1,s}\right)}\right] \Delta\left(\beta_{1,MT}\right)$$

$$+ \left[\frac{\left(\beta_{1,MT}\right)}{\left(\beta_{1,s}\right)^2}\right] \Delta\left(\beta_{1,0}\right) \tag{23}$$

$$+ \left[\frac{\beta_{MT}}{\left(\beta_{1,0}\right)^2}\right] \Delta\left(\beta_{1,0}\right)$$

Secondly, using Equation (19), we find the uncertainty of Q_s is given by

$$\Delta Q_s = \left[\frac{(\beta_{1,MT} + 1 + \beta_{2,MT})(\beta_{1,0})(\beta_{1,s})}{\Delta f(3db)(\beta_{1,MT})(\beta_{1,0} - \beta_{1,s})}\right]\Delta(f_o) \qquad (24)$$

$$+\left[\frac{f_o(\beta_{1,0})(\beta_{1,s})}{\Delta f(3db)(\beta_{1,MT})(\beta_{1,0} - \beta_{1,s})}\right]\Delta(\beta_{2,MT})$$

$$+\left[\frac{f_o(\beta_{1,MT} + 1 + \beta_{2,MT})(\beta_{1,0})^2}{\Delta f(3db)(\beta_{1,MT})(\beta_{1,0} - \beta_{1,s})^2}\right]\Delta(\beta_{1,2})$$

$$+\left[\frac{f_o(\beta_{1,MT} + 1 + \beta_{2,MT})(\beta_{1,s})^2}{\Delta f(3db)(\beta_{1,MT})(\beta_{1,0} - \beta_{1,s})^2}\right]\Delta(\beta_{1,0})$$

$$+\left[\frac{f_o(\beta_{1,0})(\beta_{1,s})(1 + \beta_{2,MT})}{\Delta f(3db)(\beta_{1,0} - \beta_{1,s})(\beta_{1,MT})^2}\right]\Delta(\beta_{1,MT})$$

$$+\left[\frac{f_o(\beta_{1,MT} + 1 + \beta_{2,MT})(\beta_{1,0})(\beta_{1,s})}{[\Delta f(3db)]^2(\beta_{1,MT})(\beta_{1,0} - \beta_{1,s})}\right]\Delta(\Delta f(3db))$$

For the case in which the sample is placed in a two-line cavity coupling system, an equation similar to (18) can be developed. In fact, we get

$$\frac{Q_W}{Q_s} = \frac{\beta_{2,MT}(\beta_{2,0} - \beta_{2,s})}{(\beta_{2,0})(\beta_{2,s})} \qquad (25)$$

Then, by using Equations (19), (20), and (25), we can develop equations similar to (21) through (24) which relate Q_s to the second coupling iris parameters, f_o and $\Delta f(3db)$.

Q_s is defined as,

$$\frac{2\pi(\text{Energy Stored in the Cavity})}{(\text{Energy Dissipated in the Sample in One Cycle})}$$

The energy stored in the cavity is equal to[16]

$$\frac{1}{2}\int_v \mu_0 H^2 \, dv$$

where H is the amplitude of the magnetic field. The energy dissipated in the sample is due to ohmic losses and in one cycle is equal to

$$\frac{\delta_s \pi \mu_s}{2}\int_s H_T^2 \, ds$$

where δ_s is the skin depth of the sample, μ_s is the permeability of the sample, H_T is the amplitude of the magnetic field parallel to the sample's surface and the integral is taken over the total surface area of the sample. Thus

$$Q_s = \frac{2\mu_0}{\delta_s \mu_s}\frac{\int_v H^2 \, dv}{\int_s H_T^2 \, ds} \tag{26}$$

As the samples are only weakly paramagnetic $\frac{\mu_0}{\mu s} = 1$ to within 0.1% Hence we use the following equation for Q_s;

$$Q_s = \frac{2\int_v H^2 \, dv}{\delta_s \int_s H_T^2 \, ds} \tag{27}$$

Using the TE mode numbers, we can find the magnetic field configuration within the cavity. Thus, Equation (27) can be solved to a good approximation, as follows:

Our coordinate system is that used in Technique of Microwave Measurements, Vol. 11 of the M.I.T. Radiation Laboratory Series, edited by C. G. Montgomery, McGraw-Hill, Inc. 1947, page 295. The dimensions of our cavity are A, parallel to the x axis, B parallel to the y axis, and C, parallel to the Z axis

With the thin sample placed in the cavity such that its corners are located at (x_1, y_1, z_0), (x_1, y_2, z_0), (x_2, y_1, z_0) and (x_2, y_2, z_0) where $z_0 = \Omega\lambda g/2$, Ω an integer, we arrive at the following solutions to Equation (27) as discussed in Appendix A:

A. If $(x_2 - x_1) \cdot (y_2 - y_1)$ which is the cross sectional area of the sample is comparable in size to $(A \cdot B)$ which is the cross sectional area of the cavity, then

$$Q_s = \frac{\pi AC[B^2p^2 + C^2]}{4\delta_s B^2p^2(x_2 - x_1)\left[\frac{\pi}{2B}(y_2 - y_1) - \frac{1}{4}\sin\left(\frac{2\pi}{B}y_2\right) + \frac{1}{4}\sin\left(\frac{2\pi}{B}y_1\right)\right]} \quad (28)$$

B. If $(x_2 - x_1) \cdot (y_2 - y_1) = \delta << (A \cdot B)$ and $(y_1 + y_2)/2 = y_0$.

$$Q_s = AC[B^2p^2 + C^2]/\delta_s(4Bp^2)\sin^2\left(\frac{\pi}{B}y_0\right) \cdot \delta \quad (29)$$

Thus we can write δ_s as a function of Q_s, the cavity geometry, the sample position, and the normal mode, all of which can be found from experimental values. Equations 28 or 29 were used to calculate the values of δ_s presented in Tables 2 and 3 of this report.

Finally, the uncertainty in δ_s is given for large samples by

$$\Delta\delta_s = \frac{\delta_s}{Q_s}\Delta Q_s + \left|\left[\frac{\pi AC[p^2B^2 + c^2]}{Q_s 4B^2p^2(x_2 - x_1)\left[\frac{\pi}{2B}(y_2 - y_1) - \frac{1}{4}\sin\left[\frac{2\pi}{B}(y_2 + \Delta y)\right] + \frac{1}{4}\sin\left[\frac{2\pi}{B}(y_1 + \Delta y)\right]\right.} - \delta_s\right]\right| \tag{30}$$

and for small samples by

$$\Delta\delta_s = \frac{\delta_s}{Q_s}\Delta Q_s + \left|\left[\frac{AC[B^2p^2 + c^2]}{Q_s 4B^2p^2 \cdot S \cdot \sin^2\left[\frac{\pi}{B}(y_0 + \Delta y)\right]} - \delta_s\right]\right| \tag{31}$$

where Δy is the uncertainty of the position of the sample along the y axis in the cavity.

Equation (31) can be used to estimate the dependence of the sensitivity of substitution techniques on flake size and skin depth. We calculate the the values of the second term (in the brackets) to pass through the 10% value for combinations such as:

δ = 25.0 microns with $\Delta x \sim \Delta y \sim 0.5$ mm

and δ = 2.5 microns with $\Delta x \sim \Delta y \sim 2$ mm

and δ = 0.25 microns with $\Delta x \sim \Delta y \sim 5$ mm

This uncertainty (by Eq. 31) rises steeply for smaller semiconductor flakes and is only a few percent, for larger ones.

APPENDIX C

CAVITY LOADING BY SEMICONDUCTOR END WALL

X = The reflective cavity with choke and the sample as an end wall

Y = The reflective cavity with choke and a flat piece of Cu as an end wall

Z = The reflective cavity with equal dimensions to X and Y but without a choke

T = The transmission cavity

$Q_{c,1}$ = The Q of the first coupling iris

$Q_{c,2}$ = The Q of the second coupling iris

$Q_{R,CH}$ = The Q of the choke joint due to microwave energy being radiated out of the slots of the choke

$Q_{w,s}$ = The Q of the sample end wall

$Q_{w,X}$ = The Q of the X cavity due to ohmic losses in the walls of the cavity except for the sample which acts as an end wall

$Q_{w,Y}$ = The Q of the Y cavity due to ohmic losses in the walls of the cavity except for the Cu flat, which acts as an end wall

$Q_{w,Z}$ = The Q of the Cu flat acting as an end wall in the Y cavity

$Q_{w,\ end}$ = The Q of the end wall of the Z cavity

$\beta_{1,\underline{\mu}}$ = The coupling parameter of the first coupling iris as measured in the $\underline{\mu}$ cavity

$\beta_{2,\underline{\mu}}$ = The coupling parameter of the second coupling iris as measured in the $\underline{\mu}$ cavity

H. Equations for cavity X

$$1B.\quad \frac{1}{Q_{c,1}} + \frac{1}{Q_{R,CH}} + \frac{1}{Q_{w,s}} + \frac{1}{Q_{w,X}} = \frac{1}{Q_{L,X}}$$

$$2B.\quad \frac{1}{Q_{R,CH}} + \frac{1}{Q_{w,s}} + \frac{1}{Q_{w,X}} = \frac{1}{Q_{u,X}}$$

$$3B.\quad \beta_{1,X}\, Q_{c,1} = Q_{u,X}$$

I. Equations for cavity Y

$$4B\quad \frac{1}{Q_{c,1}} + \frac{1}{Q_{R,CH}} + \frac{1}{Q_{w,Cu}} + \frac{1}{Q_{w,Y}} = \frac{1}{Q_{L,Y}}$$

$$5B.\quad \frac{1}{Q_{R,CH}} + \frac{1}{Q_{w,Cu}} + \frac{1}{Q_{w,Y}} = \frac{1}{Q_{u,Y}}$$

$$6B\quad \beta_{1,X}\, Q_{c,1} = Q_{u,Y}$$

J. Equations for cavity Z

$$7B.\quad \frac{1}{Q_{c,1}} + \frac{1}{Q_{w,Z}} = \frac{1}{Q_{w,Z}}$$

$$8B.\quad \beta_{1,Z}\, Q_{c,1} = Q_{w,Z}$$

K. Equations for cavity T

$$9B.\quad \frac{1}{Q_{c,1}} + \frac{1}{Q_{w,T}} + \frac{1}{Q_{c,2}} = \frac{1}{Q_{L,T}}$$

$$10B.\quad Q_{L,T} = \frac{f_o}{\Delta f(3db)}$$

$$11B.\quad Q_{w,T} = Q_{L,T}(\beta_{1,T} + \beta_{2,T} + 1)$$

In a rectangular mode $Q_{R,CH}$ is small enough that it cannot be ignored in the above equations. Therefore, a final solution to $Q_{w,s}$ must take into account the value of $Q_{R,CH}$

If we assume that $Q_{w,Z}$ is equal to $Q_{w,T}$, then, using equations 8B. and 11B. we get

$$12B. \quad Q_{c,1} = \frac{Q_{L,T}(\beta_{1,T} + \beta_{2,T} + 1)}{\beta_{1,Z}} \qquad \text{and thus,}$$

$$13B. \quad Q_{u,X} = \frac{(\beta_{1,X})Q_{L,T}(\beta_{1,T} + \beta_{2,T} + 1)}{(\beta_1, Z)}$$

also, since

$$\frac{1}{Q_{u,X}} = \frac{1}{Q_{R,CH}} + \frac{1}{Q_{w,s}} + \frac{1}{Q_{w,Y}}$$

and

$$\frac{1}{Q_{w,end}} + \frac{1}{Q_{w,X}} = \frac{1}{Q_{w,z}} \qquad \text{thus,}$$

$$14B. \quad \frac{1}{Q_{u,X}} = \frac{1}{Q_{R,Ch}} + \frac{1}{Q_{W,s}} + \frac{1}{Q_{w,Z}} - \frac{1}{Q_{w,end}}$$

As $(K)Q_{w,Z}$ is equal to $Q_{w,end}$, where K is a constart determined by the geometry of the cavity, we get

$$15B. \quad \frac{1}{Q_{u,X}} = \frac{1}{Q_{R,CH}} + \frac{1}{Q_{w,s}} - \frac{1}{(K)Q_{w,Z}} + \frac{1}{Q_{w,Z}}$$

To solve for $\frac{1}{Q_{R,CH}}$, we assume that the losses in the Cu end wall piece of cavity Y are equal to the losses in the end wall of cavity Z, so that $Q_{w,Cu}$ is equal to $Q_{w,end}$, then

16B. $\frac{1}{Q_{w,Z}} = \frac{1}{Q_{w,Cu}} + \frac{1}{Q_{w,X}}$ using equations 5B, 6B, 12B,

and 16B., we get

17B. $$\frac{1}{Q_{R,CH}} = \frac{(\beta_{1,Z})}{Q_{L,T}(\beta_{1,T} + \beta_{2,T} + 1)(\beta_{1,X})} - \frac{1}{Q_{w,Z}} .$$

Substituting 17B. into 15B. and using equations 11B. and 13B yields

18B. $$\frac{1}{Q_{w,s}} = \frac{(\beta_{1,Z})}{Q_{L,T}(\beta_{1,T} + \beta_{2,T} + 1)}\left[\frac{1}{\beta_{1,X}} - \frac{1}{\beta_{1,X}} + \frac{1}{(K)\beta_{1,Z}}\right]$$

Now $K = \frac{Q_{w,end}}{Q_{w,Z}} = \frac{\int_{sw} H_T^2 \, ds}{\int_{se} H_T^2 \, ds}$ where sw

indicates that the integral is taken over all the surface area of the cavity, se indicates that the integral is taken over the end wall only, and H_T is the magnitude of the tangential magnetic field. In fact,

$K = \frac{[2C^3A + c^3B + p^2B^3C + 2Ap^2B^3]}{AB^3p^2}$ where A, B, and C are

the dimensions of the Z cavity, and $p = \frac{2C}{\lambda g}$

Finally, as $Q_{w,s} = \frac{2\int_v H^2 \, dv}{\delta_s \int_{se} H_T^2 \, ds}$ we get

19B. $$\delta_s = \frac{[B^2p^2 + C^2]\,C}{Q_{w,s}B^2p^2} \quad \text{and}$$

$$\Delta\delta_s = \frac{[B^2p^2 + C^2]C}{B^2p^2(Q_{w,s})^2}\,\Delta(Q_{w,s}) = \frac{\delta_s}{Q_{w,s}} \cdot \Delta(Q_{w,s}).$$

APPENDIX D

GaAs PL DATA REDUCTION

(by J. M. Rowe)

A computer program has been used to aid in correcting photoluminescence data for the response of the optical system, photomultiplier tube and associated electronics. Calibration factors obtained by running a tungsten ribbon lamp and using the known emissivity of tungsten had been tabulated by wavelength every 5 Å between 8010 Å and 8920 Å and were read in by the computer. The remainder of the input consisted of chart reference marks and data points in chart coordinates, all taken from the record produced during a data run. Since the computer used data in chart paper coordinates, much work was saved.

During data taking, the wavelength in Ångstroms was noted at the beginning and end of a run and these points were marked on the chart paper. These wavelengths and their corresponding coordinates were read into the computer and using this the computer determined the wavelengths in Ångstroms of data points. This coordinate was taken as an integer for convenience. PL amplitude coordinates were taken as floating point numbers and were arbitrary to within a scale factor written down during data taking in case it would be needed later.

Each data wavelength was found in the table using linear interpolation and the interpolated correction factor applied. Corrected amplitudes were each divided by the maximum uncorrected amplitude for the data set to yield comparable scales. This was done for convenience. The scale factor appears in the printout and no information was lost. The electron volt equivalent of each wavelength was also computed.

The output appears in tabulated form with five columns. These are: (1) corrected and scaled amplitude, (2) energy in electron volts, (3) wavelength in Ångstroms, (4) uncorrected amplitude, and (5) chart coordinate of wavelength. The listing was made in order of increasing energy, or alternatively fed to Karla Dalton's program for display and for automatic graphing at the Tektronix terminal of the UNIVAC 1108 computer.

The flow chart for the PL DATA REDUCTION program is given on the next page. A listing of the program and one output table is attached, too.

FL Data Reduction Flow Chart

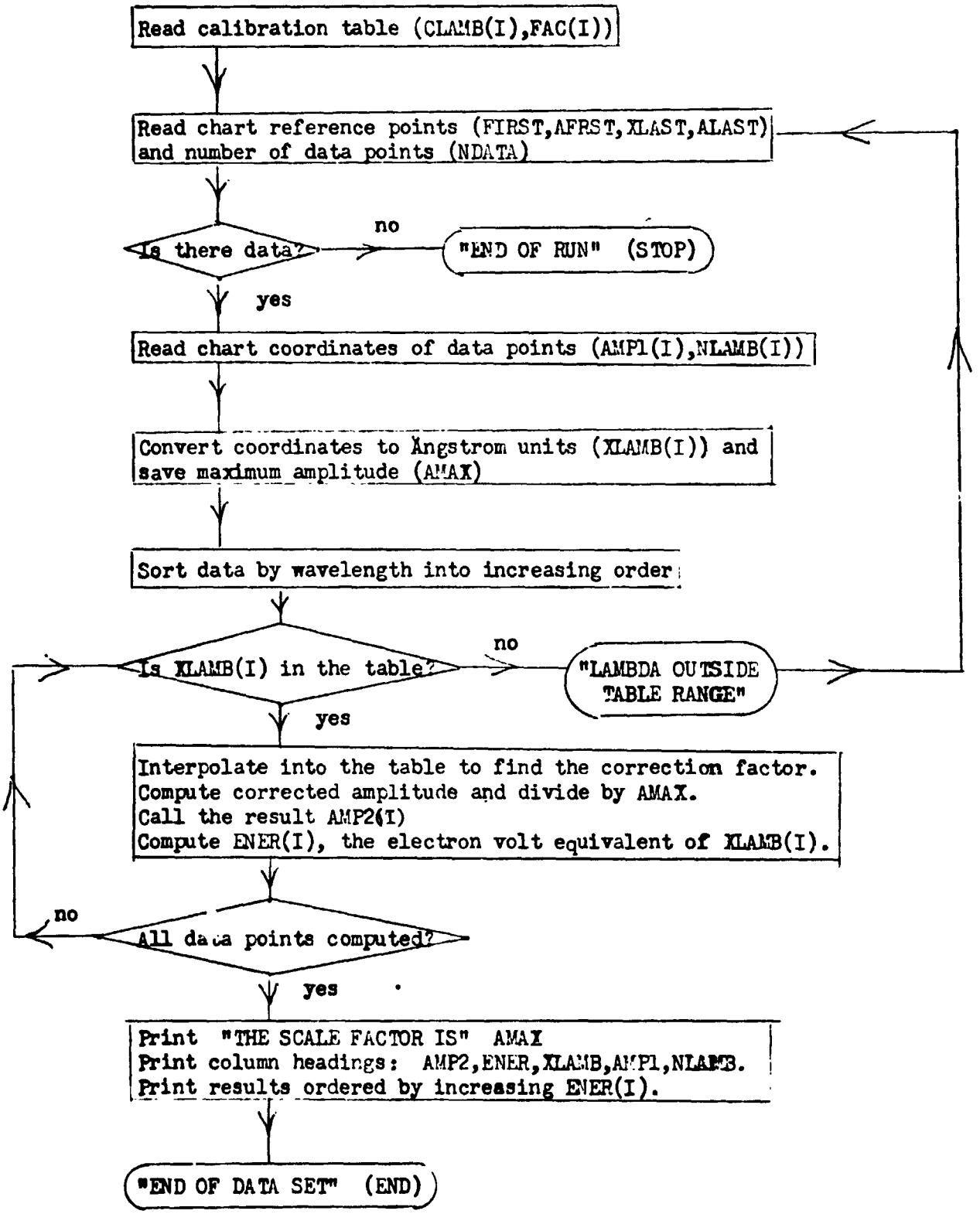

GLOSSARY (By order of appearance)

CLAMB(I)	wavelength in the calibration table
FAC(I)	calibration factor at wavelength CLAMB(I)
FIRST	wavelength (Å) of initial chart reference mark
AFRST	chart coordinate of initial chart reference mark
XLAST	wavelength (Å) of final chart reference mark
ALAST	chart coordinate of final chart reference mark
NDATA	number of data points for the chart
AMP1(I)	chart coordinate of the PL amplitude
NLAMB(I)	chart coordinate of wavelength (integer) corresponding to AMP1(I)
XLAMB(I)	wavelength (Å) corresponding to NLAMB(I)
AMAX	maximum uncorrected amplitude found in the data set
AMP2(I)	corrected amplitude divided by AMAX
ENER(I)	energy (eV) corresponding to XLAMB(I)

```
,ST
U 02/27-10:23:26-(,,)
000   @ASG,T 10,T
000   @SAVT 10,KARLADALTON CASTLE PL DATA REDUCTION
000   @ FOR,XIST  GAAS
000   C     G(A)A(S)  PL DATA REDUCTION
000         DIMENSION CLAMB(500),FAC(500),AMP1(300),NLAMB(300)
000         DIMENSION XLAMB(300),AMP2(300),ENER(300)
000      10 FORMAT (I5)
000      20 FORMAT (8F10.2)
000      25 FORMAT (4F10.2,I5)
000      30 FORMAT (F10.2,I5,F10.2,2I5)
000      40 FORMAT (F10.2,I5)
000         READ 10,ITBL
000         READ 20,(CLAMB(J),FAC(J),CLAMB(J+1),FAC(J+1),CLAMB(J+2),FAC(J+2),
000        1CLAMB(J+3),FAC(J+3), J=1,ITBL,4)
000       1 READ 25,FIRST,AFRST,XLAST,ALAST,NDATA
000         IF (NDATA.GT.0) GO TO 3
000         PRINT 90
000      90 FORMAT (1X,11HEND OF RUN.)
000         STOP
000       3 READ 40,(AMP1(J),NLAMB(J),J=1,NDATA)
000         DIFN = ALAST - AFRST
000         UNIT = (XLAST - FIRST)/DIFN
000         AMAX = AMP1(1)
000         DO 100 I = 1,NDATA
000         XLAMB(I) = (NLAMB(I) - AFRST)*UNIT + FIRST
000     100 IF (AMP1(I).GT.AMAX) AMAX = AMP1(I)
000         NDM1 = NDATA - 1
000         DO 400 I = 1,NDM1
000         IP1 = I + 1
000         DO 400 J = IP1,NDATA
000         IF(XLAMB(I).LE.XLAMB(J)) GO TO 400
000         TEMP = XLAMB(I)
000         XLAMB(I) = XLAMB(J)
000         XLAMB(J) = TEMP
000         TEMP=NLAMB(I)
000         NLAMB(I)=NLAMB(J)
000         NLAMB(J)=TEMP
000         TEMP = AMP1(I)
000         AMP1(I) = AMP1(J)
000         AMP1(J) = TEMP
000     400 CONTINUE
000         N = 1
000         DO 200 I = 1,NDATA
000         DO 300 J = N,ITBL
000         IF(XLAMB(I) .GE.CLAMB(J)) GO TO 300
000         N = J
000         C=(XLAMB(I)-CLAMB(J-1))/(CLAMB(J)-CLAMB(J-1))
000         C=C*(FAC(J)-FAC(J-1))+FAC(J-1)
000         AMP2(I)=AMP1(I)*C/AMAX
000         ENER(I) = 1.2395E4/XLAMB(I)
000         GO TO 200
000     300 CONTINUE
000         PRINT 50
000      50 FORMAT (1X,27HLAMBDA OUTSIDE TABLE RANGE.)
000         GO TO 1
```

```
000      200 CONTINUE
000          PRINT 55, AMAX
000       55 FORMAT(1X,' THE SCALE FACTOR IS ',F10.4)
000        2 PRINT 60
000          WRITE(10)NDATA,(ENER(I),AMP2(I),XLAMB(I),AMP1(I),I=1,NDATA)
000          PRINT 70 (AMP2(I),ENER(I),XLAMB(I),AMP1(I),NLAMB(I),
000         1 I = NDATA,1,-1)
000          PRINT 80
000       60 FORMAT(/7X,4HAMP2,6X,4HENER,5X,5HXLAMB,6X,4HAMP1,2X,5HNLAMB/)
000       70 FORMAT (1X,2F10.4,2F10.2,I5)
000       80 FORMAT(/1X,16HEND OF DATA SET.//)
000          END
000  $XQT
000     184
000     8010.      1.000      8015.      1.006      8020.      1.013      8025.      1.021
000     8030.      1.028      8035.      1.037      8040.      1.045      8045.      1.052
000     8050.      1.060      8055.      1.067      8060.      1.073      8065.      1.081
000     8070.      1.089      8075.      1.098      8080.      1.106      8085.      1.115
000     8090.      1.122      8095.      1.130      8100.      1.138      8105.      1.144
000     8110.      1.151      8115.      1.158      8120.      1.164      8125.      1.172
000     8130.      1.181      8135.      1.189      8140.      1.196      8145.      1.204
000     8150.      1.212      8155.      1.220      8160.      1.227      8165.      1.234
000     8170.      1.242      8175.      1.250      8180.      1.258      8185.      1.267
000     8190.      1.275      8195.      1.282      8200.      1.290      8205.      1.298
000     8210.      1.305      8215.      1.313      8220.      1.320      8225.      1.328
000     8230.      1.337      8235.      1.344      8240.      1.352      8245.      1.360
000     8250.      1.367      8255.      1.374      8260.      1.382      8265.      1.390
000     8270.      1.397      8275.      1.404      8280.      1.411      8285.      1.420
000     8290.      1.430      8295.      1.438      8300.      1.446      8305.      1.454
000     8310.      1.462      8315.      1.470      8320.      1.477      8325.      1.485
000     8330.      1.493      8335.      1.502      8340.      1.511      8345.      1.519
000     8350.      1.527      8355.      1.535      8360.      1.544      8365.      1.551
000     8370.      1.560      8375.      1.569      8380.      1.576      8385.      1.585
000     8390.      1.600      8395.      1.611      8400.      1.621      8405.      1.630
000     8410.      1.640      8415.      1.651      8420.      1.663      8425.      1.672
000     8430.      1.680      8435.      1.693      8440.      1.707      8445.      1.722
000     8450.      1.733      8455.      1.742      8460.      1.753      8465.      1.764
000     8470.      1.779      8475.      1.793      8480.      1.807      8485.      1.821
000     8490.      1.835      8495.      1.851      8500.      1.868      8505.      1.888
000     8510.      1.908      8515.      1.929      8520.      1.951      8525.      1.971
000     8530.      1.992      8535.      2.014      8540.      2.040      8545.      2.061
000     8550.      2.084      8555.      2.113      8560.      2.144      8565.      2.175
000     8570.      2.204      8575.      2.236      8580.      2.268      8585.      2.297
000     8590.      2.331      8595.      2.368      8600.      2.407      8605.      2.443
000     8610.      2.491      8615.      2.540      8620.      2.576      8625.      2.624
000     8630.      2.678      8635.      2.733      8640.      2.789      8645.      2.831
000     8650.      2.912      8655.      2.976      8660.      3.041      8665.      3.109
000     8670.      3.182      8675.      3.259      8680.      3.334      8685.      3.415
000     8690.      3.511      8695.      3.605      8700.      3.707      8705.      3.808
000     8710.      3.903      8715.      4.028      8720.      4.161      8725.      4.284
000     8730.      4.409      8735.      4.542      8740.      4.700      8745.      4.856
000     8750.      5.025      8755.      5.184      8760.      5.346      8765.      5.518
000     8770.      5.718      8775.      5.925      8780.      6.147      8785.      6.386
000     8790.      6.653      8795.      6.862      8800.      7.094      8805.      7.319
000     8810.      7.640      8815.      8.013      8820.      8.313      8825.      8.636
000     8830.      9.007      8835.      9.342      8840.      9.727      8845.     10.118
000     8850.     10.513      8855.     11.003      8860.     11.506      8865.     12.019
```

```
000  8870.   12.538   8875.   13.014   8880.   13.625   8885.   14.242
000  8890.   14.917   8895.   15.404   8900.   15.924   8905.   16.553
000  8910.   17.392   8915.   18.232   8920.   18.965
000      8792.70      2.60    8249.10     75.40    73
000        5.0    3
000        6.0    4
000        7.6    5
000        9.6    6
000       12.1    7
000       14.7    8
000       17.8    9
000       22.8   10
000       28.3   11
000       35.2   12
000       41.0   13
000       44.2   14
000       45.4   15
000       45.3   16
000       45.2   17
000       44.7   18
000       44.2   19
000       43.7   20
000       43.1   21
000       42.6   22
000       42.0   23
000       41.3   24
000       40.7   25
000       40.0   26
000       39.5   27
000       38.8   28
000       38.0   29
000       37.1   30
000       36.2   31
000       35.5   32
000       34.7   33
000       33.9   34
000       33.0   35
000       32.0   36
000       31.1   37
000       30.2   38
000       29.5   39
000       28.6   40
000       27.8   41
000       27.2   42
000       26.4   43
000       25.3   44
000       24.5   45
000       23.7   46
000       22.9   47
000       22.0   48
000       21.2   49
000       20.8   50
000       19.8   51
000       19.2   52
000       18.4   53
000       17.9   54
000       17.3   55
```

```
000        16.8     56
000        16.2     57
000        15.7     58
000        15.0     59
000        14.5     60
000        13.9     61
000        13.2     62
000        12.7     63
000        12.1     64
000        11.7     65
000        11.0     66
000        10.7     67
000        10.3     68
000         9.8     69
000         9.6     70
000         9.3     71
000         8.9     72
000         8.6     73
000         8.4     74
000         8.0     75
000
```

```
HOWE - ACCT UAHXXXXXXXXX PROJECT: QSQSQS
```